Experimental Observation of the Quantum Anomalous Hall Effect in a Magnetic Topological Insulator

Cui-Zu Chang *et al.*

Science **340**, 167 (2013);
DOI: 10.1126/science.1234414

Science (print ISSN 0036-8075; online ISSN 1095-9203) is published weekly, except the last week in December, by the American Association for the Advancement of Science, 1200 New York Avenue NW, Washington, DC 20005.

Experimental Observation of the Quantum Anomalous Hall Effect in a Magnetic Topological Insulator

Cui-Zu Chang,[1,2]* Jinsong Zhang,[1]* Xiao Feng,[1,2]* Jie Shen,[2]* Zuocheng Zhang,[1] Minghua Guo,[1] Kang Li,[2] Yunbo Ou,[2] Pang Wei,[2] Li-Li Wang,[2] Zhong-Qing Ji,[2] Yang Feng,[1] Shuaihua Ji,[1] Xi Chen,[1] Jinfeng Jia,[1] Xi Dai,[2] Zhong Fang,[2] Shou-Cheng Zhang,[3] Ke He,[2]† Yayu Wang,[1]† Li Lu,[2] Xu-Cun Ma,[2] Qi-Kun Xue[1]†

The quantized version of the anomalous Hall effect has been predicted to occur in magnetic topological insulators, but the experimental realization has been challenging. Here, we report the observation of the quantum anomalous Hall (QAH) effect in thin films of chromium-doped $(Bi,Sb)_2Te_3$, a magnetic topological insulator. At zero magnetic field, the gate-tuned anomalous Hall resistance reaches the predicted quantized value of h/e^2, accompanied by a considerable drop in the longitudinal resistance. Under a strong magnetic field, the longitudinal resistance vanishes, whereas the Hall resistance remains at the quantized value. The realization of the QAH effect may lead to the development of low-power-consumption electronics.

The quantum Hall effect (QHE), a quantized version of the Hall effect (*1*), was observed in two-dimensional (2D) electron systems more than 30 years ago (*2*, *3*). In QHE, the Hall resistance, which is the voltage across the transverse direction of a conductor divided by the longitudinal current, is quantized into plateaus of height $h/\nu e^2$, with h being Planck's constant, e the electron's charge, and ν an integer (*2*) or a certain fraction (*3*). In these systems, the QHE is a consequence of the formation of well-defined Landau levels and thus only possible in high-mobility samples and strong external magnetic fields. However, there have been numerous proposals to realize the QHE without applying any magnetic field (*4*–*11*). Among these proposals, using the thin film of a magnetic topological insulator (TI) (*6*–*9*, *11*), a new class of quantum matter discovered recently (*12*, *13*), is one of the most promising routes.

Magnetic field–induced Landau quantization drives a 2D electron system into an insulating phase that is topologically different from the vacuum (*14*, *15*); as a consequence, dissipationless states appear at sample edges. The topologically nontrivial electronic structure can also occur in certain 2D insulators with time reversal symmetry (TRS) broken by current loops (*4*) or by magnetic ordering (*6*), requiring neither Landau

[1]State Key Laboratory of Low-Dimensional Quantum Physics, Department of Physics, Tsinghua University, Beijing 100084, China. [2]Beijing National Laboratory for Condensed Matter Physics, Institute of Physics, The Chinese Academy of Sciences, Beijing 100190, China. [3]Department of Physics, Stanford University, Stanford, CA 94305–4045, USA.

*These authors contributed equally to this work.
†Corresponding author. E-mail: qkxue@mail.tsinghua.edu.cn (Q.-K.X.); kehe@iphy.ac.cn (K.H.); yayuwang@tsinghua.edu.cn (Y.W.)

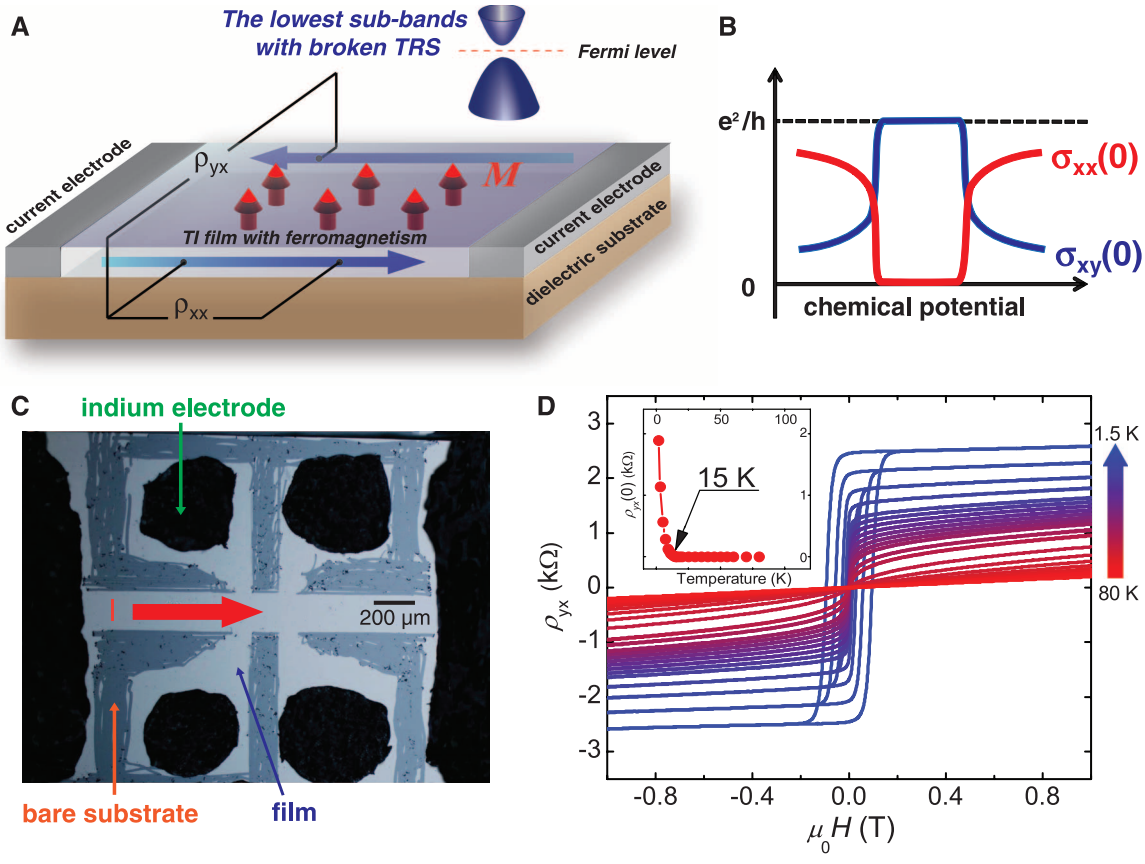

Fig. 1. Sample structure and properties. (A) A schematic drawing depicting the principle of the QAH effect in a TI thin film with ferromagnetism. The magnetization direction (M) is indicated by red arrows. The chemical potential of the film can be controlled by a gate voltage applied on the back side of the dielectric substrate. **(B)** A schematic drawing of the expected chemical potential dependence of zero field σ_{xx} [$\sigma_{xx}(0)$, in red] and σ_{xy} [$\sigma_{xy}(0)$, in blue] in the QAH effect. **(C)** An optical image of a Hall bar device made from a $Cr_{0.15}(Bi_{0.1}Sb_{0.9})_{1.85}Te_3$ film. The red arrow indicates the current flow direction during the measurements. The light gray areas are the remained film, and the dark gray areas are bare substrate with the film removed. The black areas are the attached indium electrodes. **(D)** Magnetic field dependence of ρ_{yx} curves of the $Cr_{0.15}(Bi_{0.1}Sb_{0.9})_{1.85}Te_3$ film measured at different temperatures (from 80 K to 1.5 K). The inset shows the temperature dependence of zero field ρ_{yx}, which indicates a Curie temperature of ~15 K.

levels nor an external magnetic field. This type of QHE induced by spontaneous magnetization is considered the quantized version of the conventional (nonquantized) anomalous Hall effect (AHE) discovered in 1881 (*16*). The quantized Hall conductance is directly given by a topological characteristic of the band structure called the first Chern number. Such insulators are called Chern insulators.

One way to realize a Chern insulator is to start from a time-reversal-invariant TI. These materials, whose topological properties are induced by spin-orbit coupling, were experimentally realized soon after the theoretical predictions in both 2D and 3D systems (*12*, *13*). Breaking the TRS of a suitable TI (*17*) by introducing ferromagnetism can naturally lead to the quantum anomalous Hall (QAH) effect (*6*–*9*, *11*). By tuning the Fermi level of the sample around the magnetically induced energy gap in the density of states, one is expected to observe a plateau of Hall conductance (σ_{xy}) of e^2/h and a vanishing longitudinal conductance (σ_{xx}) even at zero magnetic field [figure 14 of (*7*) and Fig. 1, A and B].

The QAH effect has been predicted to occur by Mn doping of the 2D TI realized in HgTe quantum wells (*8*); however, an external magnetic field was still required to align the Mn moments in order to realize the QAH effect (*18*). As proposed in (*9*), due to the van Vleck mechanism doping the Bi_2Te_3 family TIs with isovalent 3d magnetic ions can lead to a ferromagnetic insulator ground state and, for thin film systems, this will further induce the QAH effect if the magnetic exchange field is perpendicular to the plane and overcomes the semiconductor gap. Here, we investigate thin films of $Cr_{0.15}(Bi_{0.1}Sb_{0.9})_{1.85}Te_3$ (*19*, *20*) with a thickness of 5 quintuple layers (QL), which are grown on dielectric $SrTiO_3$ (111) substrates by molecular beam epitaxy (MBE) (*20*, *21*) (fig. S1). With this composition, the film is nearly charge neutral so that the chemical potential can be fine-tuned to the electron- or hole-conductive regime by a positive or negative gate voltage, respectively, applied on the backside of the $SrTiO_3$ substrate (*20*). The films are manually cut into a Hall bar configuration (Fig. 1C) for transport measurements. Varying the width (from 50 μm to 200 μm) and the aspect ratio (from 1:1 to 2:1) of the Hall bar does not influence the result. Figure 1D displays a series of measurements, taken at different temperatures, of the Hall resistance (ρ_{yx}) of the sample in Fig. 1C, as a function of the magnetic field ($\mu_0 H$). At high temperatures, ρ_{yx} exhibits linear magnetic field dependence due to the ordinary Hall effect (OHE). The film mobility is ~760 cm^2/Vs, as estimated from the measured longitudinal sheet resistance (ρ_{xx}) and the carrier density determined from the OHE. The value is much enhanced compared with the samples in our previous study (*20*, *21*), but still much lower than that necessary for QHE (*2*, *3*). With decreasing temperature, ρ_{yx} develops a hysteresis loop characteristic of the AHE, induced by the ferromagnetic order in the film (*22*). The square-shaped loop with large coercivity (H_c = 970 Oersted at 1.5 K) indicates a long-range ferromagnetic order with out-of-plane magnetic anisotropy. The Curie temperature is estimated to be ~15 K (Fig. 1D, inset) from the temperature dependence of the zero field ρ_{yx} that reflects spontaneous magnetization of the film.

Figure 2, A and C, shows the magnetic field dependence of ρ_{yx} and ρ_{xx}, respectively, measured at T = 30 mK at different bottom-gate voltages (V_gs). The shape and coercivity of the ρ_{yx} hysteresis loops (Fig. 2A) vary little with V_g, thanks to the robust ferromagnetism probably mediated by the van Vleck mechanism (*9*, *20*). In the magnetized states, ρ_{yx} is nearly independent of the magnetic field, suggesting perfect ferromagnetic ordering and charge neutrality of the sample. On the other hand, the AH resistance (height of the loops) changes dramatically with V_g, with a maximum value of h/e^2 around $V_g = -1.5$ V. The magnetoresistance (MR) curves (Fig. 2C) exhibit the typical shape for a ferromagnetic material: two sharp symmetric peaks at the coercive fields.

The V_g dependences of ρ_{yx} and ρ_{xx} at zero field [labeled $\rho_{yx}(0)$ and $\rho_{xx}(0)$, respectively] are plotted in Fig. 2B. The most important obser-

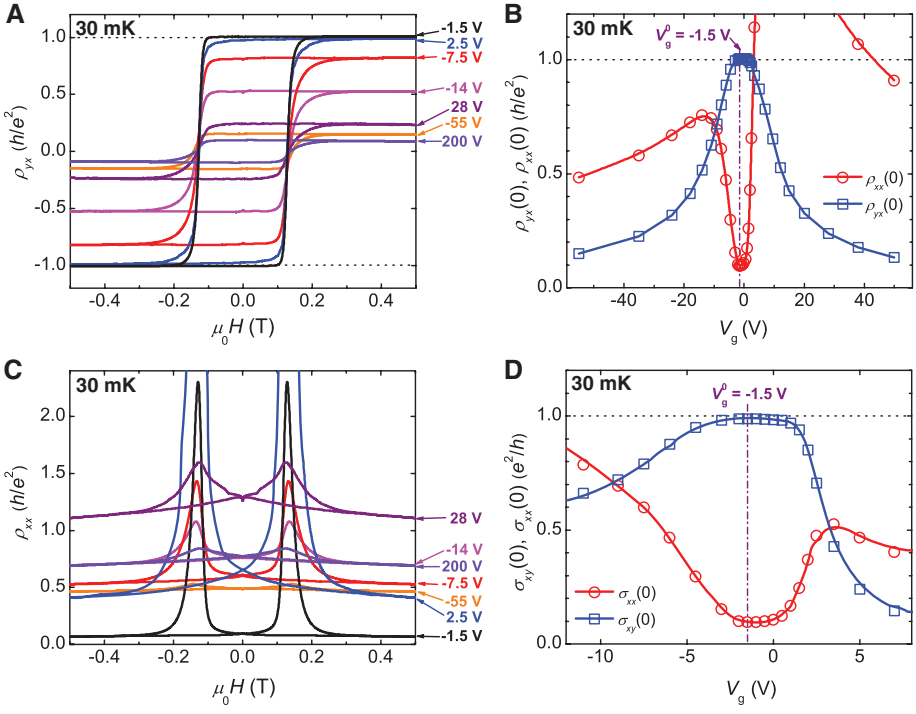

Fig. 2. The QAH effect measured at 30 mK. (**A**) Magnetic field dependence of ρ_{yx} at different V_gs. (**B**) Dependence of $\rho_{yx}(0)$ (empty blue squares) and $\rho_{xx}(0)$ (empty red circles) on V_g. (**C**) Magnetic field dependence of ρ_{xx} at different V_gs. (**D**) Dependence of $\sigma_{xy}(0)$ (empty blue squares) and $\sigma_{xx}(0)$ (empty red circles) on V_g. The vertical purple dashed-dotted lines in (B) and (D) indicate the V_g for V_g^0. A complete set of the data is shown in fig. S3.

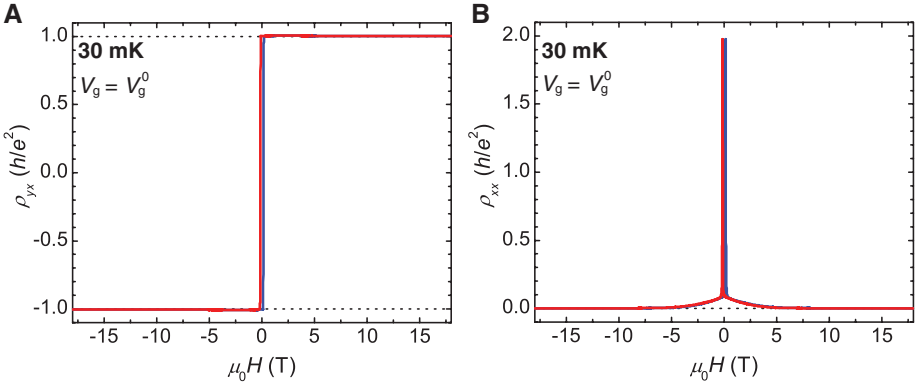

Fig. 3. The QAH effect under strong magnetic field measured at 30 mK. (**A**) Magnetic field dependence of ρ_{yx} at V_g^0. (**B**) Magnetic field dependence of ρ_{xx} at V_g^0. The blue and red lines in (A) and (B) indicate the data taken with increasing and decreasing fields, respectively.

vation here is that the zero field Hall resistance exhibits a distinct plateau with the quantized value h/e^2, which is centered around the gate voltage $V_g = -1.5$ V. This observation constitutes the discovery of the QAH effect. According to the OHE measurements, the maximum of ρ_{yx} is always located at the charge neutral point (V_g^0) (*20*, *21*). Accompanying the quantization in ρ_{yx}, the longitudinal resistance $\rho_{xx}(0)$ exhibits a sharp dip down to 0.098 h/e^2. The $\rho_{yx}(0)/\rho_{xx}(0)$ ratio corresponds to a Hall angle of 84.4°. For comparison with theory, we transform $\rho_{yx}(0)$ and $\rho_{xx}(0)$ into sheet conductance through the relations $\sigma_{xy} = \rho_{yx}/(\rho_{yx}^2 + \rho_{xx}^2)$ and $\sigma_{xx} = \rho_{xx}/(\rho_{yx}^2 + \rho_{xx}^2)$ and plot them in Fig. 2D. Around V_g^0, $\sigma_{xy}(0)$ has a notable plateau at 0.987 e^2/h, whereas $\sigma_{xx}(0)$ has a dip down to 0.096 e^2/h, similar to the behavior of the corresponding resistances.

In addition to the observation of the QAH effect, the MR ratio $\{[\rho_{xx}(H_c) - \rho_{xx}(0)]/\rho_{xx}(0)\}$ is dramatically enhanced at V_g^0 to a surprisingly large value of 2251% (Fig. 2C and fig. S3). The huge MR can also be understood in terms of the QAH phenomenology. In the magnetized QAH state, the existence of dissipationless edge state leads to a nearly vanishing ρ_{xx} (*21*). At the coercive field, the magnetization reversal of a QAH system leads to a quantum phase transition between two QH states (*7*) via a highly dissipative phase with a large ρ_{xx}, although the exact mechanism may be complex (*23*). The huge MR thus reflects the distinct difference in transport properties between an ordinary insulator and a QAH insulator.

For a QH system (*2*, *3*), when the Fermi level lies in the gap between Landau levels, σ_{xy} reaches a plateau at $\nu e^2/h$ and σ_{xx} drops to zero. If the system contains nonlocalized dissipative conduction channels, σ_{xx} has a nonzero value, whereas σ_{xy} deviates slightly from the quantized plateau (*24*). For a QAH system, only one σ_{xy} plateau of e^2/h appears at zero field when the Fermi level falls in the mobility edges around the magnetically induced gap (Fig. 1B). The observations of $\sigma_{xy}(0) = e^2/h$ plateau and the dip in $\sigma_{xx}(0)$ near the charge neutral point in Fig. 2D thus agree with the theoretical prediction for a QAH system with residual dissipative channels. The channels are expected to vanish completely at zero temperature (*11*, *24*).

To confirm the QAH effect observed in Fig. 2, we apply a magnetic field, aiming to localize all possible dissipative states in the sample. Figure 3, A and B, displays the magnetic field dependence of ρ_{yx} and ρ_{xx} of the same sample as in Fig. 2, respectively. Except for the large MR at H_c, increasing the field further suppresses ρ_{xx} toward zero. Above 10 T, ρ_{xx} vanishes completely, corresponding to a perfect QH state. It is noteworthy that the increase in ρ_{xx} from zero (above 10 T) to 0.098 h/e^2 (at zero field) is very smooth and ρ_{yx} remains at the quantized value h/e^2, which indicates that no quantum phase transition occurs, and the sample stays in the same QH phase as the field sweeps from 10 T to zero field. Therefore, the complete quantization above 10 T can only be attributed to the same QAH state at zero field.

The observation of the QAH effect is further supported by the behavior with varying temperatures. In Fig. 4A, we show V_g dependences of $\rho_{yx}(0)$ and $\rho_{xx}(0)$ measured at different temperatures in another sample with the same growth conditions. The $\rho_{yx}(0)$ always exhibits a single maximum, with the peak value considerably suppressed by increasing temperatures, accompanied by the disappearance of the dip in $\rho_{xx}(0)$. The $\sigma_{xx}(0)$ extracted from these measurements (in logarithmical scale) (Fig. 4B) exhibits a temperature dependence similar to that in integer QH systems: The drop of σ_{xx} is at first rapid, resulting from the freezing of the thermal activation mechanism, and then becomes much slower when the temperature is below 1 K. It can be attributed to variable range hopping (VRH) (*24*), but its exact mechanism remains unknown. Similar to the QHE, zero field σ_{xx} is expected to decrease to zero at sufficiently low temperature. In Fig. 4C, we plot the relation between $\sigma_{xx}(0)$ and $\delta\sigma_{xy}(0)$ ($\delta\sigma_{xy} = e^2/h - \sigma_{xy}$, which reflects the contribution of dissipative channels). A power law relation $\delta\sigma_{xy} \propto \sigma_{xx}$ with $\alpha \sim 1.55$ is obtained. For a ferromagnetic insulator in the VRH regime, the AH conductivity is related to the longitudinal conductivity through $\sigma_{AH} = A\sigma_{xx}^{\alpha}$ [the power α is ~ 1.6; the prefactor A can be positive or negative depending on materials (*22*)]. The above result can thus be qualitatively understood within the VRH framework.

Our results demonstrate the realization of the QAH effect in magnetic TIs. Compared with QHE systems, all the samples studied in this work have a rather low mobility (<1000 cm^2/Vs). Such robust QAH states not only reflect the topological character of TIs but also make the QAH systems readily achievable in experiments. Because the realization of the QAH effect and dissipationless edge states does not require any magnetic field, the present work paves a path for developing low-power-consumption, topological quantum electronic and spintronic devices.

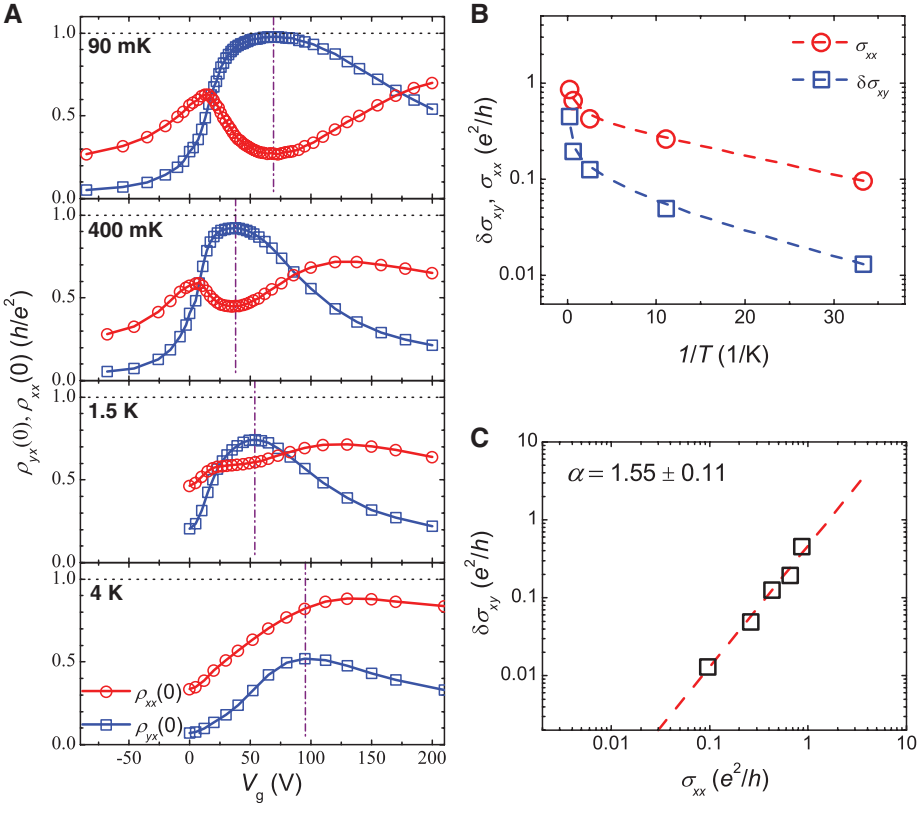

Fig. 4. Temperature dependence of the QAH effect on a different sample. (**A**) V_g-dependent $\rho_{yx}(0)$ and $\rho_{xx}(0)$ measured at 90 mK, 400 mK, 1.5 K, and 4 K, respectively. The vertical purple dashed-dotted line indicates the V_g for V_g^0. The variation in the position and width of the $\rho_{yx}(0)$ peak at different temperatures results from the change in substrate dielectric properties induced by temperature and charging cycles. (**B**) Dependences of logarithmically scaled $\sigma_{xx}(0)$ (empty red circles) and $\delta\sigma_{xy}(0)$ (empty blue squares) at V_g^0 on inverse temperature. The dashed lines are a guide to the eye. (**C**) The relation between $\delta\sigma_{xy}(0)$ and $\sigma_{xx}(0)$ at V_g^0 in double logarithmic scale. The red dashed line indicates the fit with a power law $\delta\sigma_{xy} \propto \sigma_{xx}^{\alpha}$ with $\alpha \sim 1.55$.

References and Notes

1. E. H. Hall, *Am. J. Math.* **2**, 287 (1879).
2. K. Klitzing, G. Dorda, M. Pepper, *Phys. Rev. Lett.* **45**, 494 (1980).
3. D. C. Tsui, H. L. Stormer, A. C. Gossard, *Phys. Rev. Lett.* **48**, 1559 (1982).

4. F. D. M. Haldane, *Phys. Rev. Lett.* **61**, 2015 (1988).
5. M. Onoda, N. Nagaosa, *Phys. Rev. Lett.* **90**, 206601 (2003).
6. X. L. Qi, Y. S. Wu, S. C. Zhang, *Phys. Rev. B* **74**, 085308 (2006).
7. X. L. Qi, T. L. Hughes, S. C. Zhang, *Phys. Rev. B* **78**, 195424 (2008).
8. C. X. Liu, X. L. Qi, X. Dai, Z. Fang, S. C. Zhang, *Phys. Rev. Lett.* **101**, 146802 (2008).
9. R. Yu *et al.*, *Science* **329**, 61 (2010).
10. Z. Qiao *et al.*, *Phys. Rev. B* **82**, 161414 (2010).
11. K. Nomura, N. Nagaosa, *Phys. Rev. Lett.* **106**, 166802 (2011).
12. M. Z. Hasan, C. L. Kane, *Rev. Mod. Phys.* **82**, 3045 (2010).
13. X. L. Qi, S. C. Zhang, *Rev. Mod. Phys.* **83**, 1057 (2011).
14. R. B. Laughlin, *Phys. Rev. B* **23**, 5632 (1981).
15. D. J. Thouless, M. Kohmoto, M. P. Nightingale, M. Nijs, *Phys. Rev. Lett.* **49**, 405 (1982).
16. E. H. Hall, *Philos. Mag.* **12**, 157 (1881).
17. H. Zhang *et al.*, *Nat. Phys.* **5**, 438 (2009).
18. H. Buhmann, *Bulletin of the American Physical Society* **57(1)**, P27.1 (2012), http://meetings.aps.org/link/BAPS.2012.MAR.P27.1.
19. J. Zhang *et al.*, *Nat. Commun.* **2**, 574 (2011).
20. C.-Z. Chang *et al.*, *Adv. Mater.* **25**, 1065 (2013).
21. See supplementary materials.
22. N. Nagaosa, J. Sinova, S. Onoda, A. H. MacDonald, N. P. Ong, *Rev. Mod. Phys.* **82**, 1539 (2010).
23. J. G. Checkelsky, J. Ye, Y. Onose, Y. Iwasa, Y. Tokura, *Nat. Phys.* **8**, 729 (2012).
24. B. Jeckelmann, B. Jeanneret, *Rep. Prog. Phys.* **64**, 1603 (2001).

Acknowledgments: The authors thank X. Xie, C. Yang, and X.-L. Qi for stimulating discussions and X.-C. Hong and S.-Y. Li for help with experiments. We are grateful to the National Science Foundation and Ministry of Science and Technology of China and the Chinese Academy of Sciences for financial support.

Supplementary Materials

www.sciencemag.org/cgi/content/full/science.1234414/DC1
Materials and Methods
Supplementary Text
Figs. S1 to S5
References (*25*, *26*)

21 December 2012; accepted 1 March 2013
Published online 14 March 2013;
10.1126/science.1234414

Evidence for Two Distinct Populations of Type Ia Supernovae

Xiaofeng Wang,[1,2]* Lifan Wang,[2,3] Alexei V. Filippenko,[4] Tianmeng Zhang,[5] Xulin Zhao[1]

Type Ia supernovae (SNe Ia) have been used as excellent standardizable candles for measuring cosmic expansion, but their progenitors are still elusive. Here, we report that the spectral diversity of SNe Ia is tied to their birthplace environments. We found that those with high-velocity ejecta are substantially more concentrated in the inner and brighter regions of their host galaxies than are normal-velocity SNe Ia. Furthermore, the former tend to inhabit larger and more luminous hosts. These results suggest that high-velocity SNe Ia likely originate from relatively younger and more metal-rich progenitors than do normal-velocity SNe Ia and are restricted to galaxies with substantial chemical evolution.

Type Ia supernovae (SNe Ia) are among the most energetic and relatively uniform stellar explosions in the universe and were used to discover its accelerating expansion (*1*, *2*). They are thought to originate from a thermonuclear explosion of an accreting carbon-oxygen (C-O) white dwarf (WD) near the Chandrasekhar mass limit [$M_{Ch} \approx 1.4$ solar mass ($M_\odot$)] in a close binary system (*3*, *4*). Two competing scenarios have been proposed for the progenitor systems: single-degenerate (SD) (*5*, *6*) and double-degenerate (DD) models (*4*, *7*). In the former, the mass-donating star could be a main-sequence (MS)/subgiant star (*8*), a red-giant star (RG) (*9*), or even a helium star (*10*, *11*), whereas it is another WD in the latter scenario (*4*, *7*). Recent results suggest that both scenarios are possible (*12*–*18*).

There is increasing evidence for spectral diversity among SNe Ia. Of particular interest are those showing higher expansion velocities as inferred from the blueshifted Si II 615-nm feature in optical spectra (*19*). These fast-expanding SNe Ia also generally exhibit a steep Si II temporal velocity gradient (*20*). This spectral difference in velocity or velocity evolution of the ejecta has been proposed to be a geometric effect of an asymmetric explosion (*21*, *22*). Given a common origin for SNe Ia having different ejecta velocities, they should be found in similar stellar environments. This can be tested by examining SN positions in their hosts, the surface brightness at these locations, and the properties of their hosts.

We conducted such an analysis with a well-defined SN sample having 188 SNe Ia (supplementary text S1) from the Lick Observatory Supernova Search (LOSS) (*23*). The SN Ia sample consists of 123 "Branch-normal" (spectroscopically normal) objects (*24*), 30 peculiar ones of the SN 1991bg variety (*25*), 13 peculiar ones such as SN 1991T (*26*, *27*), and 7 peculiar ones such as SN 2002cx (*28*), with respective fractions of 65.4, 16.0, 6.9, and 3.7% (table S1). There are 15 SNe Ia (8.0% of all) that cannot be subclassified because of an absence of early-time spectra. We concentrated on the Branch-normal SNe Ia, which are thought to be relatively uniform. We obtained the main parameters of the host galaxies from two large online astronomical databases: the NASA/Infrared Processing and Analysis Center (IPAC) Extragalactic Database (NED) (*29*) and HyperLeda (*30*).

The location of a SN in its host galaxy can be estimated by the radial distance of the SN from the nucleus (R_{SN}). Assuming that the galaxies are circular disks and only appear to have different major and minor axes because of their inclination, R_{SN} can be calculated if we know the position angle and the axial ratio of each galaxy. The radius of the galaxy (R_{gal}) is simply the semi-major axis at the 25.0 *B*-mag arc sec^{-2} isophote. The ratio R_{SN}/R_{gal} is then the fractional radial distance of the SN. For SNe Ia in elliptical galaxies, no tilt correction is applied because these galaxies can be regarded as spheroids. The typical host galaxy of our sample (fig. S1) has a major axis of about 1.3′ to 1.4′ and can be measured with a precision of ~0.1′. This results in a typical uncertainty of ~0.05 in the determination of R_{SN}/R_{gal}.

We measured the velocity of the Si II 615-nm line for 165 SNe Ia (out of 188) by using the published spectral data sets (*31*–*33*). We normalized this velocity to the maximum-light value with a series of templates of Si II velocity evolution established from well-observed SNe Ia, with a typical uncertainty of 300 to 400 km s^{-1} (supplementary text S1 and fig. S2).

It is clear that Branch-normal SNe Ia with $v_{Si\ II} < 12{,}000$ km s^{-1} [the normal-velocity group (NV)] span a wide radial distribution, occurring at places from the innermost region to about two to three times the optical radius of the entire galaxy. In contrast, those with $v_{Si\ II} \geq 12{,}000$ km s^{-1} [the high-velocity group (HV)] are rarely found at large galactic radii (Fig. 1B). For example, only 3 out of the 40 HV SNe Ia are detected in regions with $R_{SN}/R_{gal} > 0.7$ (two of which are in elliptical galaxies), whereas 14 ± 2 would have been expected at the detection rates of the NV SNe Ia (which are about $34 \pm 5\%$ at $R_{SN}/R_{gal} > 0.7$). Such a difference has a statistical significance of about 5σ, highlighting the paucity of HV SNe Ia in outskirts of galaxies. Binning the data in velocity space with an interval of about 2000 km s^{-1} further shows a correlation between the ejecta velocity of SNe Ia and the locations in their host galaxies (Fig. 1A, gray quadrangles).

To better understand such a birthplace versus ejecta-velocity relation for SNe Ia, it is important to know how the Si II velocity itself is distributed. Most of the sample of Branch-normal SNe Ia clusters at velocities between 10,000 and 12,000 km s^{-1} (Fig. 1C), with a tail extending up to ~16,000 km s^{-1}. Such a velocity distribution can be fit by a double-Gaussian model. One com-

[1]Department of Physics, Tsinghua University, Beijing 100084, China. [2]Mitchell Institute for Fundamental Physics and Astronomy, Texas A&M University, College Station, TX 77843, USA. [3]Purple Mountain Observatory, Nanjing, 201008 Jiangsu, China. [4]Department of Astronomy, University of California, Berkeley, CA 94720–3411, USA. [5]National Astronomical Observatory of China, Chinese Academy of Sciences, Beijing 100012, China.

*Corresponding author. E-mail: wang_xf@mail.tsinghua.edu.cn